Numerical study of a 20W class QCW pulsed sodium guide star laser's performances at five sites in China

Hong-Yang Li[1,3], Lu Feng[1], Jun-Wei Zuo[2], Qi Bian[2], Bo-Tian Sun[4], Sui-Jian Xue[1], Zhi-Xia Shen[1], Yang-Peng Li[1] and Yong Bo[2]

[1] CAS Key Laboratory of Optical Astronomy, National Astronomical Observatories, Chinese Academy of Sciences, Beijing 100101, China; *Jacobfeng@bao.ac.cn, lihongyang@nao.cas.cn*
[2] Technical Institute of Physics and Chemistry, Chinese Academy of Sciences, Beijing 100190, China
[3] University of Chinese Academy of Sciences, Beijing 100049, China
[4] Department of Physics, University of California, Santa Barbara, CA 93106, USA

Abstract   In the past few years, Chinese astronomical community is actively testing astronomical sites for several new optical/infrared ground-based telescopes. These site testing campaigns conducted were mainly focused on fundamental performances of the sites, such as cloud coverage, seeing, temperature, etc. With increasing interests in sodium laser guide star adaptive optics for these new telescopes in the Chinese astronomical community, it is interesting to investigate the performance of the laser guide star at these sites, especially considering that the sodium laser guide star's on-sky performance is significantly influenced by sites' local performances, such as geomagnetic field, sodium layer dynamics, density of air molecule, etc. In this paper, we studied sodium laser guide star's performance of a 20W class Quasi Continuous Wave (QCW) pulsed laser developed by TIPC with numerical simulation for five selected sites in China.

Key words: instrumentation: adaptive optics — methods: numerical — site testing

1 INTRODUCTION

As a subsystem of Adaptive Optics (AO) system, sodium laser guide star system can provide a stable and reliable reference source for telescopes' AO systems to correct atmospheric turbulence (Hardy 1998). Sodium laser guide star systems have been utilized in most of those highly-productive large ground-based telescopes, such as the Keck Telescope (Chin et al. 2016), the European Southern Observatory's (ESO) Very Large Telescope (Calia et al. 2014), the twin Gemini Telescopes, the Gran Telescopio CANARIAS (GTC) *et cetera*, and such systems are also designed in the first place for those next generation 30 m class ground-based telescopes, such as the Thirty Meter Telescope, the European Extremely Large Telescope (E-ELT) and the Giant Magellan Telescope (GMT).

One of the most important future astronomical projects within the Chinese astronomical community, the 12 m diameter Large Optical/infrared Telescope (LOT) is also planned to have an AO system installed as soon as the telescope is constructed (Feng et al. 2020). By far, several excellent candidate sites for this large telescope and several smaller telescopes to be built in near future have been investigated in the western part of China, such as Tibet, Xinjiang, Qinghai, Sichuan, etc (Feng & Hao 2020). Site monitoring scientists have made great efforts in evaluating fundamental astronomical performances of these sites, including cloud coverage, seeing, meteorological parameters, precipitical water vapor, *et cetera* (Liu et al. 2012, 2015, 2016; Yao et al. 2013; Qian et al. 2015; Wang et al. 2015; Wu et al. 2016), but performances relating to sodium laser guide star's on-sky performances at these candidate sites, like the geomagnetic field, sodium layer dynamics and so on, are not being monitored due to the difficulties and costs for such measurements. Therefore, we investigated the performance of sodium guide star at certain typical sites in China in advance using our model combining with data from remote sensing satellites as well as other atmospheric models, to quantify the influence of some parameters related to sites on the performance of sodium guide star, such as geomagnetic field and sodium layer dynamics. The results of this study may shed lights on the future application of sodium guide stars in the western part of China.

For comparative simulation study for the on-sky performance of sodium Laser Guide Star (LGS), we

selected five sites for this study: Ali, Lenghu, Muztagh Ata, Gaomeigu in western China and Xinglong (an important site in eastern China) as a comparison. Figure 1 shows the location of the five sites. The Ali site is located in the southwest of Tibet autonomous region with an altitude of 5100 m. It is one of the three candidate sites for the 12-meter LOT (Yao et al. 2013). The Muztagh Ata site is also one candidate site for LOT, which is located in the Pamir Plateau, in the southwest of Xinjiang Province of China, and more information about the site can be seen from Xu et al. (2020). The Lenghu site is the site for the future 2.5 m Wide Field sky Survey Telescope (WFST) and it is located in the northwest border of Qaidam Basin with an average altitude of 2800 m. The Gaomeigu site is located in Lijiang, Yunnan province with an altitude of 3200 m, which has the largest general-purpose optical telescope, Lijiang 2.4-meter Telescope (LJT), in China. The Xinglong site, located at the highest latitude among the selected sites, has a history of more than 50 years and possesses two important astronomical observation instruments, the LAMOST and the 2.16 m Telescope.

The laser that we chose to simulate in this study is a 20W Quasi Continuous Wave (QCW) pulsed laser from the Technical Institute of Physics and Chemistry (TIPC) with whom we have been cooperating both in experiments and simulation study of sodium laser guide star for years. Significant amount of lab/field tests data have been gathered (Wei et al. 2012; Jin et al. 2014; Otarola et al. 2016; Bian et al. 2016a,b, 2017, 2020), and were used to verify our model previously (Jin et al. 2015; Feng et al. 2016). Although we are confident that our model would be suitable to predict LGS generation performances for other types of sodium laser, such as Continuous Wave (CW) laser, macro-micro pulsed laser (Li et al. 2021), we would like to present prediction results for such lasers at different sites until sufficient field test results have been gathered to verify our model.

In the rest of this paper, we will describe parameters related to the laser and sites in Section 2, and the simulation results will be presented in Section 3.

2 METHOD

In this paper, we used a simulation tool called Photon Return Simulation program (PRS) (Feng et al. 2015; Jin et al. 2015; Li et al. 2021) to predict the on-sky performance of 20W Quasi-CW pulse laser at aforementioned sites in China. The simulation is a Monte Carlo simulation based on rate equation. During the simulated time period (for example 1 s), the state of each atom under the influence of laser light field as well as other different physics such as geomagnetic field influence, light pressure, D2b repumping are being tracked for every 30 nanosecond. The sampling time is short enough to simulate a 100 μs QCW

Table 1 Laser Parameters for TIPC 20 Watt Quasi-CW Pulsed Sodium Laser

Parameter name	Value
Center wavelength	589.159 nm
Linewidth	~ 0.3 GHz
Longitudinal mode interval	~ 225 MHz
Longitudinal mode width (FWHM)	5 MHz
Pulse repetition rate	600 Hz
Pulse width	~ 100 μs
Average power	20 W
Polarization	circular
D2b repumping factor	15%

laser pulse. We simulate this one second process repeatedly for about 100 thousand times, which is sufficient for the result of the Monte Carlo simulation to converge and to calculate the mean value of coupling efficiency as in the Lidar equation as a representative for each laser power density. After that, we could obtain the coupling efficiency versus the projected on-sky power density curve. In this section, we will introduce the sources and values of these parameters.

2.1 The Parameters of TIPC Laser

The spectrum and pulse format of sodium laser plays an important role in predicting the return flux of sodium guide star (Kibblewhite 2000). As described previously, the laser investigated in our study is a 20W quasi-CW pulse laser from TIPC. Main parameters of the laser are summarized in Table 1. The spectrum and single pulse format of the laser are shown in Figure 2. The central wavelength of the laser is at sodium D2a line, 589.159nm, which corresponds to 0 MHz in Figure 2. The Full Width Half Maximum (FWHM) of the spectrum is about 0.3 GHz. The spectrum of the laser contains several longitudinal modes and the distances between adjacent longitudinal modes are equal which is about 225 MHz.

2.2 Sodium Atom Column Density

Photon return number is closely related to the sodium atom column density in mesosphere, while the sodium Vertical Column Density (VCD) will change obviously with latitude (Langowski et al. 2017). We utilize the empirical formula of sodium column density proposed by Fussen, which is based on remote sensing data from GOMOS (Fussen et al. 2004, 2010). The satellite is designed for measuring column densities of molecules or atoms including sodium atom in the atmosphere. Its results are further explored to show the variation of the sodium VCD with different latitudes and different months. Based on these data, Fussen formed an empirical formula of sodium column density against location and month as shown in Equation (1). In this equation, N represents sodium density for a certain month m (January is m=0)

Fig. 1 The location of the five sites in China (Xinglong, Lenghu, Muztagh Ata, Ali and Gaomeigu).
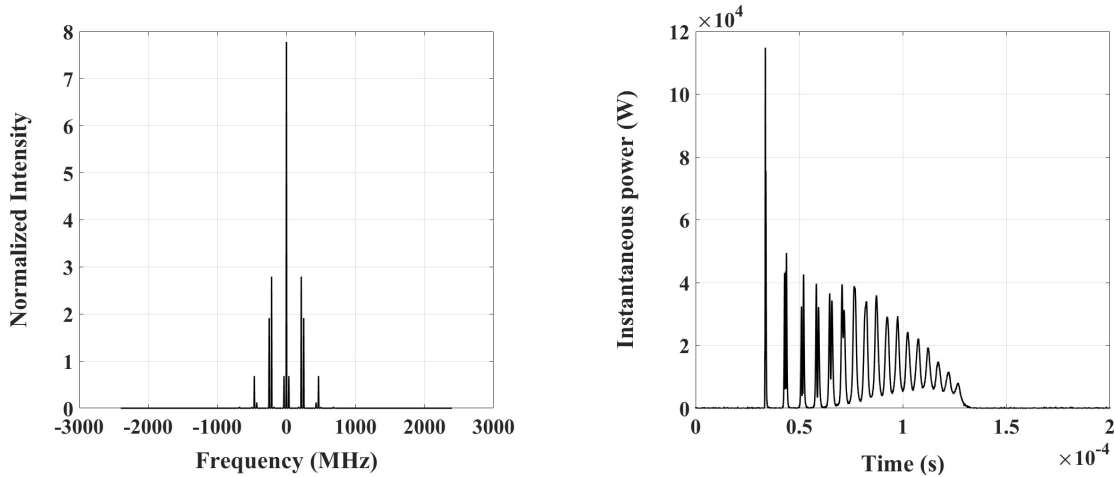
Fig. 2 Spectrum format and single pulse format of TIPC 20W Quasi-CW pulse laser. (*left*) The width (FWHM) of spectrum is 300 MHz and the width (FWHM) for each longitudinal modes is 5 MHz. (*right*) The 100 μs single pulse format of the laser.

and latitude ϕ (in radians for Eq. (1)). Other parameters in Equation (1) are listed in Table 2. According to this formula, we calculated the sodium column density in the mesosphere in different months in China for the latitude ranging from 15°N to 55°N , and the detailed results are visualized from Figure 3(left). In general, the sodium column density is higher in winter and lower in summer at the same latitude. With the increase of latitude, it increases in winter and decreases in summer, so the difference between the two seasons raises with latitude.

The sodium VCD reaches the highest in November, the lowest in May or June at the selected sites in China, as shown in Figure 3(right). The differences of sodium VCD between winter and summer are relatively large. For example, even for Gaomeigu site-the site with smallest annual difference among the sites-the sodium VCD is 87.9% higher in November than in June: in November, it can reach 4.1×10^{13} (atoms/m²), whereas in June, it is only 2.2×10^{13} (atoms/m²). Moreover, the difference of the sodium VCD between different sites is relatively large from November to January next year, while the difference between June and October is very small.

$$N(m,\phi)[\text{cm}^{-2}] = t_0 + t_1 \cos(\frac{2\pi}{12}m + t_2)$$
$$+ t_3(\phi + \frac{\pi}{2})(\phi - \frac{\pi}{2})\cos(\frac{2\pi}{6}m + t_4), \quad (1)$$
$$t_{i \leq 1} = f_i(a_0 + a_1\phi + a_2\phi^2 + a_3\phi^3),$$
$$t_0 = 3.28 \times 10^9.$$
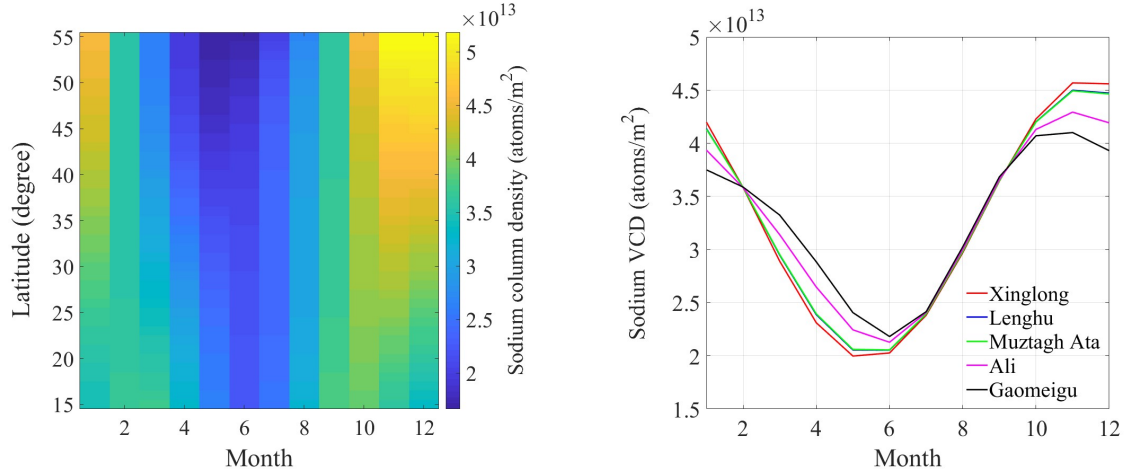
Fig. 3 (*left*) Sodium column density changes with month and latitude (15 °N–55 °N) in China and is basically higher in winter and lower in summer. (*right*) Five typical sites' sodium column density varies with month. The densities at Lenghu and Muztagh Ata are almost the same, so the curves almost coincide.

Table 2 Parameters for Equation (1)

i	f_i	a_0	a_1	a_2	a_3
1	1×10^9	0.1282	1.549	0.1780	0.03511
2	1	0.4017	0.8216	–0.1282	–0.2980
3	1×10^9	–0.2630	0.1121	0.6355	–0.3566
4	1	–1.5635	–3.0526	1.3802	1.7637

2.3 The Effect of Geomagnetic Field

The Larmor precession caused by the geomagnetic field will result in the M state of sodium atoms to change periodically with time (Moussaoui et al. 2008, 2009). The period depends on the strength of the geomagnetic field and the angle between the pointing direction of the laser and the geomagnetic field vector. Since the transition cross section of the sodium atom is different when it is at different M ground state, the periodical shift due to Larmor precession will cause a degradation of the overall coupling efficiency for LGS generation. The strength and direction of the geomagnetic field vector will change with the location of the site. The coupling efficiency and photon flux will change accordingly. This will lead to some differences in the coupling efficiency and photon return number at these sites, so it is necessary to determine the strength and direction of the geomagnetic field at these sites. In Table 3, we listed the sites' local geomagnetic field information, including declination/inclination angle and the strength of the geomagnetic field vector, which is from the World Magnetic Model (WMM).

The pointing direction of laser will change as the telescope tracks the observation target. Therefore, the angle between the laser and the geomagnetic field will also change accordingly. In our study, we evaluate the on-sky performance variation due to geomagnetic field effects. When we were analyzing the on-sky performance with different projected laser power for different months,
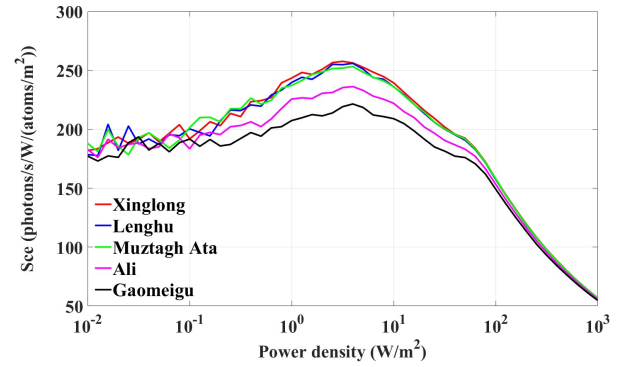
Fig. 4 Coupling efficiency against projected power density on sky (92 km) in zenith direction.

we only simulate in the zenith direction because of two reasons: 1. to easily compare with LGS field tests, since for these field tests, the projected power is deliberately varied to check against model prediction, and it is normally only conducted in the zenith without any requirement for complex laser transfer optics for pointing mechanism; 2. to simplify the calculation process. Only when discussing the annual mean on-sky performance in different directions, we performed the simulation for all five sites with the full power of the laser at 20W for all elevation/azimuth angle combinations.

2.4 Temperature and Atmospheric Molecular Density

Atmosphere molecular density and temperature in the mesosphere will influence the collision possibility between sodium atoms and atmospheric molecules/atoms and then affect the coupling efficiency and the photon return number (Kibblewhite 2000, 2008). The values of the two parameters are related with the location of a site and

Table 3 Parameters Related to Sites

Site	Latitude	Longitude	Altitude	Declination (+E | -W)	Inclination (+D | -U)	Strength of local geomagnetic field (nT)
Xinglong	40.39°N	117.58°E	960 m	−7.05°	59.33°	5.20×10^4
Lenghu	38.45°N	93.20°E	2800 m	3.58°	57.99°	5.22×10^4
Muztagh Ata	38.28°N	74.90°E	4526 m	3.56°	57.99°	5.03×10^4
Ali	32.31°N	80.05°E	5100 m	1.61°	50.33°	4.80×10^4
Gaomeigu	26.71°N	100.03°E	3200 m	−1.11°	41.59°	4.61×10^4
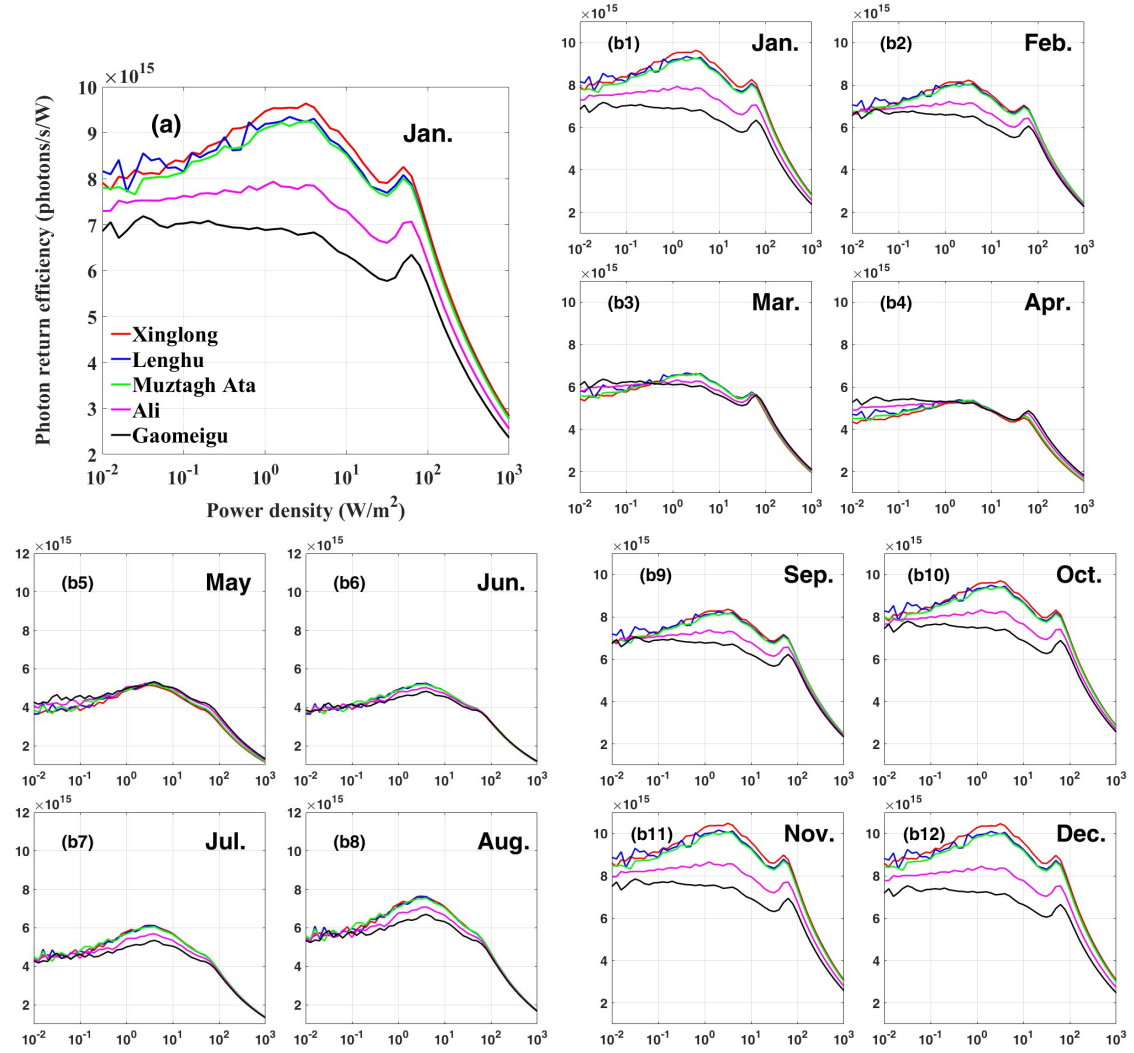
Fig. 5 Photon return efficiency variation against power density on sky (92 km) from Jan. to Dec. (b1–b12).

can be obtained by querying MSISE-90 model from the Community Coordinated Modeling Center (CCMC).

3 RESULTS

3.1 Coupling Efficiency Variation under Circular Polarization at the Zenith

The coupling efficiency of circularly polarized light is higher than that of linearly polarized light due to the larger scattering cross section of the circular polarization. For this reason, all LGS lasers are circularly polarized. In the simulation we take circular polarization as a default to simulate the performance of the TIPC laser.

The comparison of the coupling efficiencies at the zenith with different power densities is shown in Figure 4. The range of power density on sky (X-axis) is from 0.01 to 1000 W m^{-2} and the Y-axis is the coupling efficiency. The curves of different colors represent the variations of coupling efficiency against projected power densities at
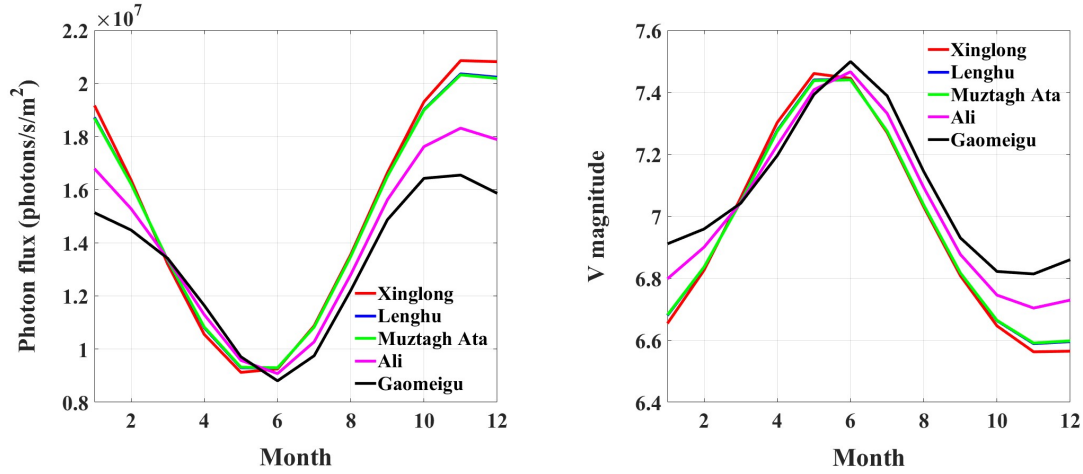
Fig. 6 Photon flux variation with month (*left*) and corresponding seasonal distribution of *V*-band magnitude of sodium laser guide star (*right*).

Table 4 Numerical Information about Coupling Efficiency (* Mean Coupling Efficiency in All Directions)

| Site	The elevation angle of the maximum coupling efficiency	Mean coupling efficiency * (photons/s/W/ (atoms/m^2))	V magnitude of the mean coupling efficiency	Maximum coupling efficiency (photons/s/W/ (atoms/m^2))	Minimum coupling efficiency (photons/s/W/ (atoms/m^2))	Elevation and azimuth angle of minimum coupling efficiency
Xinglong	60°	218.3	6.904	325.3	177.2	(El:30° Az:330°)
Lenghu	60°	217.5	6.908	327.2	177.4	(El:30° Az:40°)
Muztagh Ata	60°	218.9	6.901	325.5	178.7	(El:30° Az:340°)
Ali	50°	216.1	6.915	326.1	181.4	(El:30° Az:50°)
Gaomeigu	40°	212.1	6.935	328.7	182.5	(El:30° Az:50°)

different sites. Coupling efficiencies at Xinglong, Lenghu and Muztagh Ata are almost identical, which are higher than Ali and Gaomeigu. This is mainly due to the influence of the geomagnetic field. When the direction of laser and geomagnetic field vector is parallel, Larmor precession caused by the geomagnetic field effect is the least; when the two is vertical, the influence of Larmor precession is the strongest. From Table 3, we can see that the angles of geomagnetic field and the zenith at the former three sites are almost the same, and the geomagnetic field strength is similar. Both of them are higher than that of the latter, which explains why the coupling efficiency of Ali and Gaomeigu at zenith is lower.

3.2 Photon Return Efficiency in Zenith

In the zenith direction, the sodium column density in the mesosphere will change with month and latitude of the site, and the coupling efficiency will change with the location of sites and power density. Therefore, we use the product of the sodium column density and the coupling efficiency to investigate the change of the photon return number with the power density in different months at different sites. We temporarily call the product of the two as the photon return efficiency in zenith.

Such photon return efficiencies from January to December are shown in Figure 5. Figure 5(a) shows the photon return efficiency variation with the power density on sky in January. The curves with different colors represent the efficiencies for different sites, which are the same as in Figure 4. Figure 5(b1)–(b12) shows the change of photon return efficiency from January to December and the ranges of value for Y axis in these figures are the same for easy comparison. We can summarize Figure 5 as follows:

– In different months, the photon return efficiency of a site varies greatly. For example, the maximum photon return efficiency of Xinglong in November is 129% higher than that in June: in June, the photon return efficiency is 4.65×10^{15} (photons/s/W), but in November is 10.65×10^{15} (photons/s/W). This is mainly caused by the large change of sodium column density with the month;

– In spring and summer (from March to August), the photon return efficiencies of different sites are similar and at a low level. While in autumn and winter (from September to February), there is large differences between the photon return efficiency of five sites. The higher the latitude of site, the higher the photon return efficiency. There are two main reasons for

Xinglong

Lenghu

Muztagh Ata

Ali

Gaomeigu
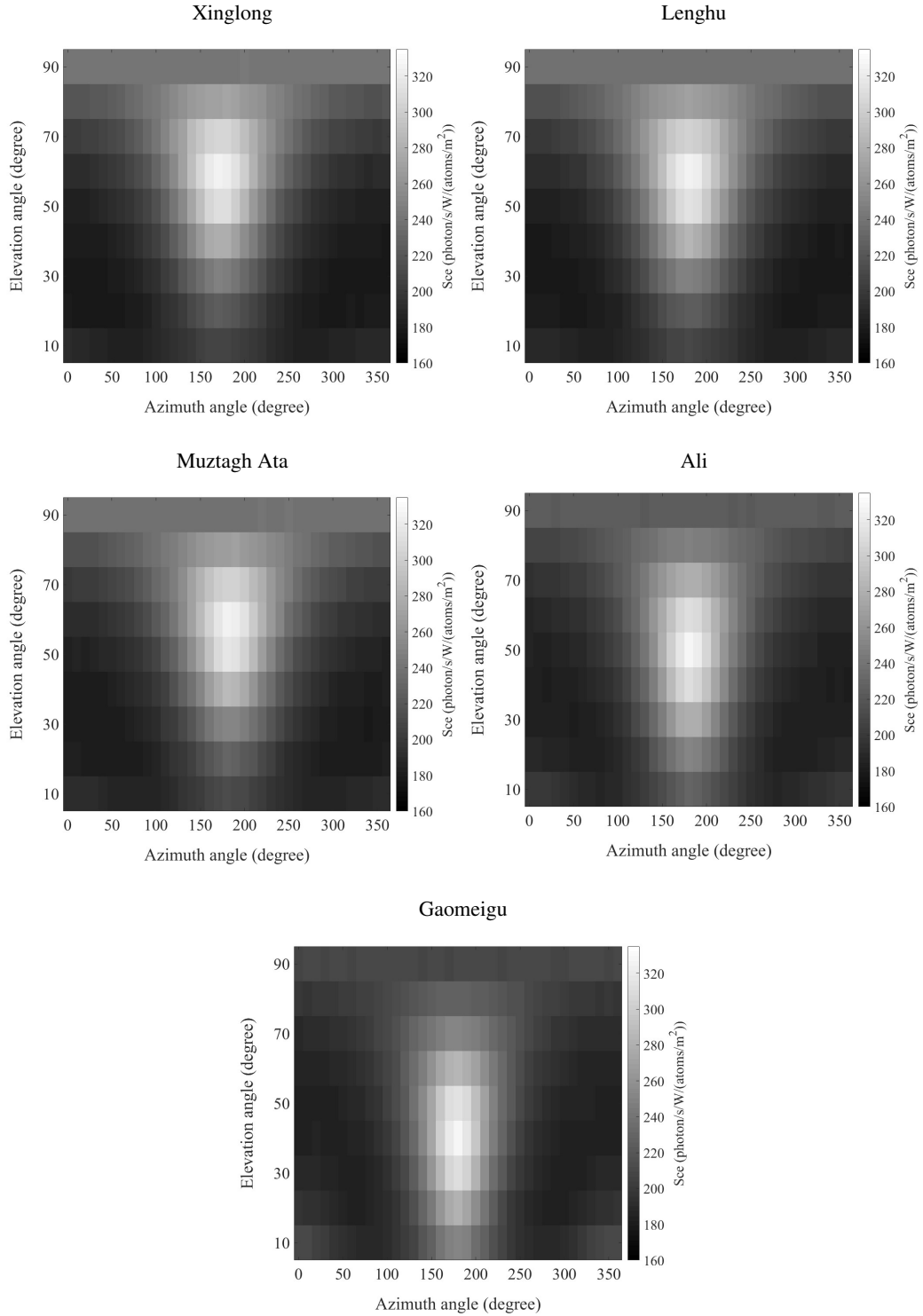
Fig. 7 Coupling efficiency distribution across the sky.

this phenomenon: one is that the coupling efficiency increases with latitude of site due to the influence of the geomagnetic field; the other is that the sodium column density keeps at high level in autumn and winter.

3.3 Returned Photon Flux

The returned photon flux determines how much photons could reach the telescope, which is exactly what astronomers are most concerned about. The relationship between the coupling efficiency and the photon flux can be described by Equation (2) from Holzlöhner's paper

(Holzlöhner et al. 2010), where Sce is the coupling efficiency, Φ is the photon flux received by the telescope (unit photons/s/m^2), L is the vertical distance from the primary of the telescope to the sodium layer, P is the laser power, T is the atmospheric transparency, $X = 1/(\sec(\theta))$ and θ is the laser launch zenith angle, C_{Na} is the sodium column density. Assuming that the atmospheric transparency at zenith is 90%, the seeing is $1.5''$ and beam quality (M^2) of TIPC laser is 1.4, the diameter of laser spot size at 92 km on sky is about $0.737\,\mathrm{m}(1.652'')$, and the mean power density at zenith is about 42.2 W m^{-2}. The coupling efficiency can be obtained from the curve of the coupling efficiency against power density (Fig. 4). According to Equation (2), the photon flux in zenith for different months can be calculated, as shown in Figure 6 (left). In general, the photon flux is higher in winter and lower in summer, and the flux variations at Xinglong, Lenghu and Muztagh Ata are identical and higher than that of Ali and Gaomeigu, which is more pronounced in winter. This is mainly due to the influence of the seasonal distribution of the sodium layer column density. According to the relationship of photon flux and magnitude of an object (Astronomical Magnitude Systems: *https://www.cfa.harvard.edu/ ~dfabricant/huchra/ay145/mags.html*), we calculated the corresponding Johnson V-band magnitude variation of the sodium guide star with month, shown in Figure 6 (right). The highest V magnitude is up to 6.56 in November at Xinglong and the lowest is about 7.50 in June at Gaomeigu.

$$\Phi = \frac{Sce \cdot P \cdot (T)^{2X} \cdot C_{Na} \cdot X}{L^2} . \qquad (2)$$

3.4 Coupling Efficiency Variation with Direction of the Laser

As mentioned in the previous section, during an astronomical observation, the direction of laser guide star would change with the pointing direction of a telescope. Thus, the angle between the laser direction and the local geomagnetic field vector will change, and this will cause continuous change of coupling efficiency because of the varying influence of the geomagnetic field. In addition, for slanted pointing directions, the increasing airmass will reduce both the projected laser power and the return photon flux. Therefore, the coupling efficiency has a peculiar spatial distribution on sky with different pointing directions. In this case, we conducted our simulation with a constant 20 W laser output power. For every laser pointing direction, we calculated the angle between the laser and the geomagnetic field vector, and applied this value into our simulation along with projected power density and size of spot due to airmass and slanted projection. The atmospheric transparency for every site is assumed to be

90%. The calculated on-sky coupling efficiency results are shown in Figure 7.

In each picture of Figure 7, the X-axis represents the change of the azimuth angle, with the true north at 0° and the east at 90°. The Y-axis represents the change of the elevation angle, with the horizontal direction at 0° and the zenith at 90°. The variation of the coupling efficiency with the laser direction at can be summarized as follows:

– The coupling efficiency is almost symmetric along 180° of azimuth angle. When the azimuth angle changes from north to south (0°–180°), the coupling efficiency increases gradually and then decreases when the azimuth angle changes from south to north (180°–360°);
– The coupling efficiency increases first and then decreases with the increase of elevation angle, but the elevation angles of the maximum coupling efficiency are different among the sites;
– In Xinglong, Lenghu and Muztagh Ata, the coupling efficiency reaches maximums of 325.3, 327.2 and 325.5 (photons/s/W/(atoms/m^2)) at elevation angle of 60° and azimuth angle of about 180°; In Ali, the coupling efficiency reaches a maximum of 326.1 (photons/s/W/(atoms/m^2)) at elevation angle of 50° and azimuth angle of about 180°. In Gaomeigu, the coupling efficiency reaches a maximum of 328.7 (photons/s/W/(atoms/m^2)) at elevation angle of 40° and azimuth angle of about 180°. Statistics of the results are summarized in Table 4. The mean coupling efficiency is the average in all directions, and the sodium column density is adopted the average of 12 months when we calculate the corresponding V magnitude of mean coupling efficiency.

4 CONCLUSION

In this paper, we have studied the performance of sodium laser guide stars generated by a 20W class quasi-CW pulsed laser at five typical sites of China. From Table 4, the overall annual mean performances of sodium guide star at these sites are very similar, and the similarity can be summarized as due to that the brightness of the guide star is strongly relying on the seasonal variation of sodium column density and laser pointing direction rather than geographical locations. However, for AO design concerns, coupling efficiency's variation in different months with different pointing angles are more important because it determines the performance that the AO system could function in specific night of year at a particular angle. The seasonal photon flux distribution of LGS shows higher value in winter and lower in summer. The photon return in summer is only about 44% (at Xinglong site) – 53% (at Gaomeigu site) of that in winter (see Fig. 6), which renders

a difference of 0.882–0.685 in *V* magnitude. For different laser pointing direction, the coupling efficiency changes most significantly with the azimuth angle at elevation angle from 40°to 60°. In addition, the variation of coupling efficiency with elevation angle is also prominent, which shows that the elevation angle for the maximum coupling efficiency is higher with increasing latitude as shown in Figure 7 and Table 4. With both effects combined, the variation of sodium LGS's brightness is not negligible in AO system's design process. We hope that this work could shed light on future applications of sodium laser guide star.

References

Bian, Q., Bo, Y., Zuo, J. W., et al. 2020, Optics Letters, 45, 1818

Bian, Q., Bo, Y., Zuo, J. W., et al. 2016, Optics Letters, 41, 1732

Bian, Q., Zuo, J. W., Guo, C., et al. 2016, Laser Physics, 26, 095005

Bian, Q., Zong, Q. S., Chang, J. Q., et al. 2017, IEEE Photonics Technology Letters, 29, 2095

Calia, D. B., Hackenberg, W., Holzlöhner, R., et al. 2014, Advanced Optical Technologies, 3, 345

Chin, J. C. Y., Wizinowich, P., Wetherell, E., et al. 2016, Proc. SPIE, 9909, 99090S

Feng, L., Shen, Z. X., Xue, S. J., et al. 2016, RAA (Research in Astronomy and Astrophysics), 16, 144

Feng, L., Kibblewhite, E., Jin, K., et al. 2015, Proc. SPIE, 9678, 96781B

Feng, L., Hao, J. X., Cao, Z. H., et al. 2020, RAA (Research in Astronomy and Astrophysics), 20, 080

Feng, L., & Hao, J. X. 2020, RAA (Research in Astronomy and Astrophysics), 20, 79

Fussen, D., Vanhellemont, F., Bingen, C., et al. 2004, Geophys. Res. Lett., 31, L24110

Fussen, D., Vanhellemont, F., Tétard, C., et al. 2010, Atmospheric Chemistry & Physics, 10, 9225

Hardy, J. W. 1998, Adaptive Optics for Astronomical Telescopes (New York: Oxford Univ. Press)

Holzlöhner, R., Rochester, S. M., Calia, D. B., et al. 2010, A&A, 510, A20

Jin, K., Wei, K., Feng, L., et al. 2015, PASP, 127, 749

Jin, K., Wei, K., Xie, S., et al. 2014, Proc. SPIE, 9148, 91483L

Kibblewhite, E. J. 2000, in Laser Guide Star Adaptive Optics for Astronomy, eds. Ageorges, N. & Dainty, C. (Kluwer Academic Publishers), 51

Kibblewhite, E. J., 2008, Proc. SPIE, 7015, 70150M

Langowski, M. P., Savigny, C., Burrows, J. P., et al. 2017, Atmospheric Measurement Techniques, 10, 2989

Li, H. Y., Feng, L., Wang, J. L., et al. 2021, PASP, 133, 034502

Liu, L. Y., Yao, Y. Q., Vernin, J., et al. 2012, in Proc. of SPIE, 8444, 844464

Liu, L. Y., Yao, Y. Q., Vernin, J., et al. 2015, Journal of Physics: Conference Series, 595, 012019

Liu, Y., Song, T. F., Zhang, X. F., et al. 2016, in Proc. of IAU, 320, Solar and Stellar Flares and their Effects on Planets, 447

Moussaoui, N., Holzlöhner, R., Hackenberg, W., et al. 2008, Proc. SPIE, 7015, 70152W

Moussaoui, N., Holzlöhner, R., Hackenberg, W., et al. 2009, A&A, 501, 793

Otarola, A., Hickson, P., Gagné, R., et al. 2016, Journal of Astronomical Instrumentation, 5, 1

Qian, X., Yao, Y. Q., Wang, H. S., et al. 2015, Publication of Korean Astronomical Society, 30, 695

Wang, H. S., Yao, Y. Q., Liu, L. Y., et al. 2015, Journal of Physics: Conference Series, 595, 012037

Wei, K., Bo, Y., Xue, X. H., et al. 2012, Proc. SPIE, 8447, 84471R

Wu, N., Liu, Y., & Zhang, H. M. 2016, AcASn, 57, 729

Xu, J., Esamdin, A., Hao, J. X., et al. 2020, RAA (Research in Astronomy and Astrophysics), 20, 86

Yao, Y. Q, Wang, Y. P., Liu, L. Y., et al., 2013, in NARIT Conf. Ser., 1, the 11th Asian-Pacific Regional IAU Meeting 2011, ed. Komonjinda, S. (IAU), 1, *http://conference.narit.or.th/ncs/APRIM2011_proceedings/S7/S7P05.pdf*